Effect of High Magnetic Field on Logic Gate Transfer Characteristics with Application to SEU Testing

Awipi, M., Tennessee State Univ., Engineering

In previous work, we have measured the shifts in the current-voltage characteristics of transistors of various technologies. We have extended our effort by measuring the shifts in the voltage transfer characteristics of logic gates, also of various technologies. These shifts are expected to lower noise margins, and hence, increase logical error rates of digital integrated circuits. Further, by comparing the amount of shift caused by various intensities of magnetic field to the amount of shift caused by various doses of ionizing radiation, we expect to calibrate the two effects so that magnetic fields can replace ionizing radiation in Single Event Upset (SEU) Testing of integrated circuits. In the figure, we show the shift for a 7402 TTL NOR gate with output driving one TTL inverter. The two input leads of the NOR gate are tied together for it to function as an inverter. The effect shown is for magnetic fields from 4 T to 8 T.

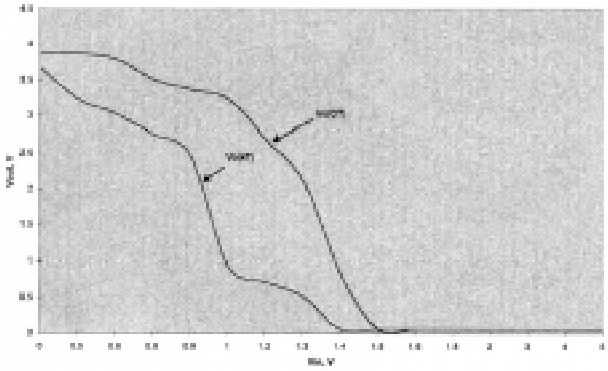

Figure 1. 7402 voltage transfer characteristic under high magnetic fields.

This work was supported by NASA Grant NCCW-0086, subgrant S700012.

Study of Spin and Charge Fluctuations in the U-t-t' Model

Buhler, C., NHMFL
Moreo, A., NHMFL/FSU, Physics and MARTECH

As additional neutron scattering experiments are performed on a variety of high temperature superconducting compounds, it appears that magnetic incommensuration is a phenomenon common to all of the samples studied. The newest experimental results indicate that incommensurate peaks exist at momentum $q=\pi(1,1\pm\delta)$ and $\pi(1\pm\delta,1)$ in $La_{2-x}Sr_xCuO_4$ (LSCO) and $YBa_2Cu_3O_{7-\delta}$ (YBCO). The dependence of δ with hole doping appears to be similar in both materials. In addition, new ARPES data for LSCO as a function of doping shows that its Fermi surface is qualitatively similar to the one of YBCO, contrary to what was previously believed. Early theoretical attempts to explain the behavior of LSCO and YBCO usually relied on one- or three-band Hubbard models, or the t-J model with electron hopping beyond nearest neighbor, and with different parameter values for each material. In this paper it is shown that using a one band Hubbard U-t-t' model with U/t=6 and $t'/t\approx-0.25$, good agreement is obtained between computational calculations, and *both* neutron scattering and ARPES experiments for LSCO and YBCO. It is also shown that using a more negative t'/t will induce short-range magnetic incommensuration along the diagonal direction in the Brillouin zone, in qualitative disagreement with the experimental results. At the finite temperatures of the present Monte Carlo simulation it is also observed that in this model the tendency to incommensurate appears to be more related to the shape of the two-dimensional Fermi surface, and the strength of the interaction, rather than to charge order.

The Ferromagnetic Kondo Model for Manganites: Phase Diagram, Charge Segregation, and Influence of Quantum Localized Spins

Dagotto, E., NHMFL/FSU, Physics and MARTECH
Yunoki, S., NHMFL
Malvezzi, A., NHMFL
Moreo, A., NHMFL/FSU, Physics and MARTECH
Hu, J., NHMFL
Capponi, S., Univ. Paul Sabatier, France
Poilblanc, D., Univ. Paul Sabatier, France
Furukawa, N., ISSP, Univ. of Tokyo

The phase diagram of the ferromagnetic Kondo model for manganites was recently investigated using computational techniques by Yunoki, *et al*., Phys. Rev. Lett. 80, 845 (1998). In dimensions 1, 2, and ∞ and using classical localized spins, this study suggested a rich low temperature phase diagram with three dominant regions: (1) a ferromagnetic phase, (2) phase separation between hole-undoped antiferromagnetic and hole-rich ferromagnetic domains, and (3) a phase with incommensurate spin correlations. The purpose of the present paper is two-fold: (a) a variety of computational results are here provided to substantiate and supplement the previous results by Yunoki, *et al*., investigating a complementary region of couplings and densities; and (b) studies using the Lanczos algorithm and the Density Matrix Renormalization Group method applied to chains with localized spin 1/2 (with and without Coulombic repulsion for the mobile electrons), and spin 3/2 degrees of freedom are discussed. The overall conclusion is that using fully quantum mechanical localized spins in one-dimensional systems, the phase diagram of the model is similar to the result obtained using classical t_{2g} spins. This result provides support to the use of classical localized spins in more complicated problems, such as in dimensions larger than one and/or including phononic and orbital degrees of freedom, where the use of classical spins is crucial to simplify the complexity of the problem.[1]

Reference:

1 Dagotto, E., *et al*., Phys. Rev. B, 58, 6414-6427 (1998).

De Haas-van Alphen Measurements on SrB_6, CaB_6, and $Ca_{0.995}La_{0.005}B_6$

Hall, D., NHMFL
Young, D., NHMFL
Fisk, Z., NHMFL
Goodrich, R.G., Louisiana State Univ., Physics

The Fermi surfaces of three materials have been measured with a quasi-steady field torque magnetometer. The measurements were carried out at temperatures between 25 and 600 mK and at fields as high as 30 T. All samples were measured with the <100> axis approximately parallel to the applied field. Fourier analysis of the measured Landau quantum oscillation data shows several frequencies for each material. SrB_6 displayed a strong oscillation at a frequency of ~48 T, with another higher frequency of ~308 T emerging at fields above 14 T. One clear oscillation ~45 T is observed in CaB_6 with two smaller peaks ~24 and ~96 emerging from the FFT. Calculations of the CaB_6 Fermi surface indicate that orbits of 24, 39,

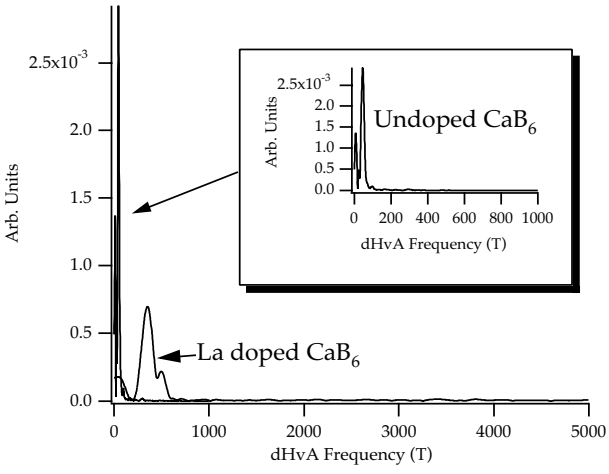

Figure 1. dHvA spectrum of doped and undoped CaB_6.

60, and 76 T should be present.[1] Finally, we investigated the affect of La doping on the Fermi surface of CaB_6. Substituting 0.5% La for Ca introduces two new, higher frequencies into the dHvA spectrum: ~350 T and ~495 T. The 45 T orbit still has the largest amplitude, but it is greatly reduced from the pure CaB_6 case. Doping a larger percentage of La for Ca destroys the dHvA signal completely. For example at 1% La doping no signals are observed. In CaB_6, La acts as a charged impurity and increases the electron scattering rate. One of the most striking results concerning these measurements is that all of the materials have large resistivities; for SrB_6 the resistivity at temperatures below 1 K is above 45 x 10^3 μΩ cm.[2]

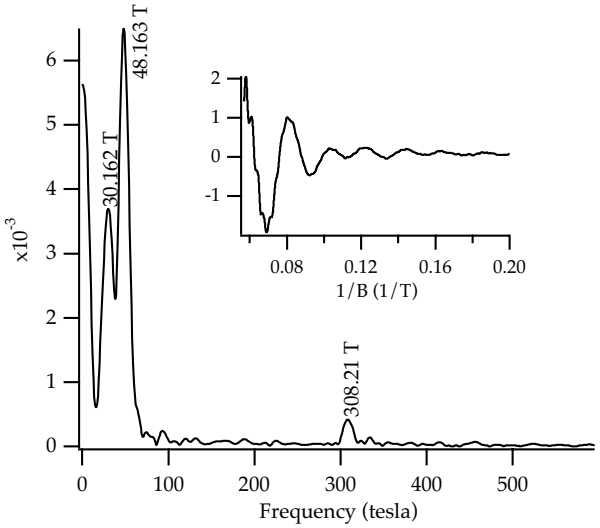

Figure 2. dHvA spectrum of SrB_6. Inset shows raw data.

References:

1 Chen, J., Hershfield, S., Sharifi, F. (private communication).

2 Ott, H.R., *et al*. Z. Phys. B, 102, 337 (1997).

Electronic Transport in a Metal with Tortuous Channels

NHMFL

Hebard, A.F., UF, Physics/NHMFL
Arnason, S.B., UF, Physics/NHMFL
Hershfield, S.P., UF, Physics/NHMFL

In a continuation of work reported last year, we have further studied electronic transport in thin Ag films having a microstructure dominated by Ag islands close to critical coalescence. By using in situ monitoring techniques during deposition, we are able to fabricate films in which electronic transport takes place in channels/paths defined by the coalescing islands and having a width comparable to or less than the transport mean free path. In this regime, the channel walls rather than impurities in the channels dominate scattering. Two important observations have been made.[1] Firstly, anomalously high resistivity scales ensue because of large geometric corrections, and secondly, a classical magnetoresistance with negative sign results because in a magnetic field the tortuous paths allow electrons to flow with less interaction with the channel walls than would be the case in zero field. This latter effect has not previously been recognized and may play an important role in understanding "novel" materials where current paths are determined by how the material is put together rather than what it is made of.

To support the conclusions inferred from the transport data, we have developed atomic force scanning probe techniques in which images of film topography together with electric potential

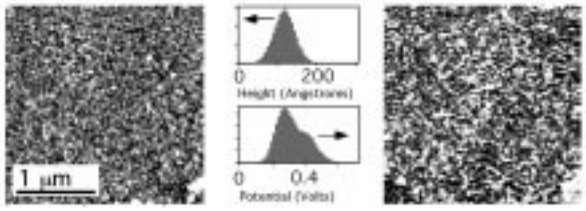

Figure 1. Topographical (left) and surface potential (right) images of a coalescing Ag film near the percolation transition.

differences can be simultaneously acquired. The technique employs an atomic force microscope, which is operated in the noncontact mode with the cantilever driven near resonance by a piezo drive. An electric potential applied at a lower frequency between the tip and the sample produces a modulation in the force with amplitude proportional to the surface potential on the film. Figure 1 shows simultaneous scans of topology (left panel) and surface potential (right panel) of a coalescing silver film. The bimodal distribution seen in the potential map reveals information about the electrical properties that can not be seen in the topographical image. We are presently improving upon this characterization technique by using carbon nanotube-modified tips and have obtained surface potential images with 100 Å spatial and 15 mV vertical resolution.

Reference:

1 Arnason, S.B., *et al.*, Phys. Rev. Lett. 81, 3936(1998).

Magnetoresistance of $BaVS_3$

Lawrence, J., Univ. of California-Irvine, Physics and Astronomy
Booth, C., LANL

The compound $BaVS_3$ has a phase transition at T_{mi} = 70 K from a high temperature metallic state to a low temperature insulating state. The susceptibility $\chi(T)$ follows a Curie law at high temperature, indicative of nearly-localized V d^1 electrons. There is a sharp peak in $\chi(T)$ at T_{mi}, and at lower temperature the susceptibility saturates to a finite value. There is no observable change in the crystal structure at the transition, and there is no magnetic long-range order in the low temperature state. The nature of the magnetism in the low temperature state, and its relation to the metal-insulator transition, remains an open question.[1]

To learn more about the low temperature magnetism, we measured the magnetoresistance of a needle shaped single crystal of $BaVS_3$ in the 20 T continuous magnet at the NHMFL-Los Alamos, during March 1998. The basic idea was to measure the effect of a magnetic field on the metal-insulator phase transition, i.e. determine $\Delta T_{mi}/\Delta H$. To accomplish this, we measured the field dependence of the resistance for a number of fixed temperatures above T and below T_{mi}. This was done for two orientations of the magnetic field, parallel and perpendicular to the needle's axis. We found that the magnetoresistance varied as H^2, and was essentially independent of field orientation. We found that if we plotted $\Delta\rho(H)/\rho(0)$ at fixed H (e.g. H = 10 T), versus temperature in the vicinity of T_{mi}, then the resulting curve varied proportionally with the quantity $(1/\rho)d\rho/dT$ measured in zero field. Using the formulas

$$\Delta\rho(H)/\rho(0) = \Delta T_{mi}(H)\,(1/\rho)d\rho/dT \quad (1)$$

and

$$\Delta T_{mi}(H) = \alpha H^2 \quad (2)$$

we then determined the quantity α to be approximately -2.0×10^{-3} K/T^2.

Under the assumption that the phase diagram is elliptic

$$(T_{mi}(H)/T_0)^2 + (H/H_0)^2 = 1 \quad (3)$$

then for T_0 = 70 K and for the value of α given above, we obtained an estimate for the zero temperature critical field, H_0 = 187 T. This is an extremely large critical field. If we assume that H_0 is the field required to Zeeman-split the energy gap, then we see that there is an order of magnitude agreement with the measured energy gap (500 K).[1]

In any case, the magnetic field has only a very small effect on the metal-insulator transition. This rules out that the transition is similar to that of a Kondo Insulator, where the magnetic field has a much larger effect. It suggests that the transition may involve an as-yet-unobserved charge density wave, since the magnetic field has only a minor effect on CDW phase transitions.

Reference:

1 Graf, T., *et al.*, Phys. Rev. B, 51, 2037 (1995).

Far-Infrared, Millimeter-Wave and Transport Studies of "Colossal" Magnetoresistance Materials

Lewis, R.A., Univ. of Wollongong, Australia, Engineering Physics
Brooks, J.S., NHMFL/FSU, Physics
Wang, Y., NHMFL
Biskup, N., NHMFL
Stalcup, T., NHMFL
Hill, S., Montana State Univ., Physics
Mola, M., Montana State Univ., Physics

Far-infrared reflectivity measurements were made on $La_{0.7}Ca_{0.3}MnO_3$ and $La_{0.8}Li_{0.2}MnO_3$ (Wang *et al.* 1998a, 1998b)[1,2] at 4.2 K and at fields of 0, 5, 10 and 15 T. The three principal spectral features evident at ambient conditions, namely the "external," "bending," and "stretching" modes (Lewis *et al.* 1998)[3] were observed, but were much suppressed at the low temperature. The application of magnetic field did not produce appreciable change in these modes, in contrast to expectation. A "transmission line" geometry was attempted in order to measure pseudo-transmission on these highly reflecting samples; this method, however, proved unviable. In contrast, good transmission data was obtained for two semiconductor samples: cyclotron resonance was observed in a 2DEG to 17.5 T and impurity transitions in GaAs:Be to the same field; it is expected that these results will form the basis of publications. Measurements were made on several materials with the MVNA apparatus. The temperature and field dependences of the mm-wave response of $(ET)_2KHg(SCN)_2$, both in the center-post and cavity-base geometries, were measured. This organic conductor showed almost identical behavior to $(ET)_2TlHg(SCN)_2$, demonstrating that the behavior first observed in the latter material is not unique to it, but may be universal. The superconducting nitride ZrNCl, which, with Tom Stalcup had earlier been measured in magnetotransport to 30 T, was also examined. The ac magneto-conductivity mirrored the field behavior of the dc conductivity—namely, an initial increase to about 10 T, then a flattening off. Both $La_{0.7}Ca_{0.3}MnO_3$ and $La_{0.8}Li_{0.2}MnO_3$ were measured in magnetotransport confirming the previously reported behavior. In the mm-wave cavity, both materials exhibit magneto-resonances, which have not, to our knowledge, been observed before in these materials. Analysis of this most recent data is continuing.

References:

1 Wang, X.L., *et al.*, J. Appl. Phys., 83, 7177 (1998a).
2 Wang, X.L. *et al.*, Phys. Rev., 58, in press (1998b).
3 Lewis, R.A., *et al.*, Aust. J. Phys., in press (1998).

Circular Current and an Additional Magnetic Moment in Ultra-Pure Metal Single Crystals

Marchenkov, V.V., Institute of Metal Physics, Ekaterinburg, Russia
Hall, D.W., NHMFL
Stalcup, T.F., NHMFL
Brooks, J.S., NHMFL/FSU, Physics

In Refs. 1 and 2, we reported on the observation of a dc voltage at the potential and hall leads, when an ac current flowed through a pure tungsten and molybdenum single crystals. Figure 1 shows a schematic view of a pure metal in an external magnetic field. One can see that electron-surface scattering moves the centers of the electron orbits to the opposite directions near the opposite sample surfaces, i.e. a circular current $j_{c.c.}$ and an additional magnetic moment may appear (Figure 1).

Pure and dirty tungsten crystals with residual resistivity ratios (RRR) of 80,000 and 800, respectively, as well as molybdenum crystals with RRR of up to 30,000 were used. We measured the dc voltage U_{dc} and an ac-susceptibility, when an

ac current with a frequency of up to $3 \cdot 10^3$ Hz flowed through the sample at temperatures from 1.5 to 30 K and in magnetic fields up to 24 T.

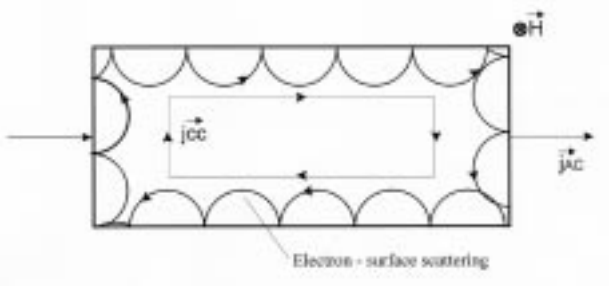

Figure 1. Circular current $j_{c.c.}$ and an additional magnetic moment resulting from electron-surface scattering near a surface of pure metal in an external magnetic field.

We proposed the following. If a circular current and an additional magnetic moment really occur, their magnitude and direction, and, hence, the magnitude, polarity and direction of measured dc voltage U_{dc} and magnetic moment M, should depend on the volume and on the direction of the external magnetic field. Besides, the appearance of U_{dc} and M has to depend on the mean free path of the conduction electrons *l*, i.e. they will occur for pure crystals at helium temperatures, when $l \geq d$ (*d* is a cross dimension of sample), and will decrease and disappear either for pure samples at temperatures about 30 K or for dirty ones at any temperatures when $l << d$.

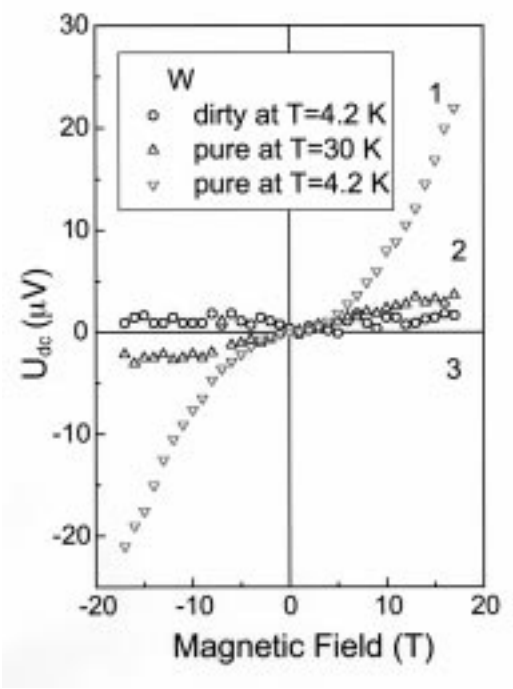

Figure 2. Field dependence of the dc voltage U_{dc} for pure (1,2) and dirty (3) tungsten crystals at different temperatures.

Figure 2 shows the field dependence of the dc voltage U_{dc} for pure tungsten at 4.2 K (1) and at 30 K (2), and for dirty tungsten at 4.2 K (3). We observed a dc voltage at the potential leads of pure sample (1), which changes its sign with the change of field direction. Decreasing the mean free path *l* either by introducing impurities into the sample (3) or by increasing the temperature up to 30 K for pure crystal (2) leads to a disappearance of the circular current and of U_{dc} (Figure 2). The similar field dependence of an additional magnetic moment M = f (B) was observed. As in the case of U_{dc} , we found that M occurs under strong electron-surface scattering and is absent at higher temperatures, when $l << d$.

References:

1 Marchenkov, V.V., *et al*., in Non-Linear Electromagnetic Systems, eds. V. Kose and J. Sievert, IOS Press, p. 815 (1998).

2 Marchenkov, V.V., *et al*., Physical Phenomena at High Magnetic Fields-III Conf. Handbook, p. 230 (1998).

Dislocation Breakdown in Tungsten and Molybdenum Single Crystals at High Magnetic Fields

Marchenkov, V.V., Institute of Metal Physics, Ekaterinburg, Russia
Stalcup, T.F., NHMFL
Brooks, J.S., NHMFL/FSU, Physics
Weber, H.W., Atomic Institute of the Austrian Universities, Vienna
Levit, V.I., NASA Langley Research Center
Kaufman, M.J., UF, Materials Science Engineering

Dislocations, i.e. linear lattice defects, always exist in real crystals and, hence, the electron-dislocation scattering will affect the electronic transport of metals. The role of electron-dislocation scattering

in the electroresistivity of metals without magnetic field was studied in many experimental and theoretical papers. Until now, however, only a few articles address the role of this scattering mechanism in an external magnetic field.[1] We wish to emphasize that some characteristic peculiarities of the electron-dislocation interaction may manifest themselves only in a magnetic field. For example, no experimental confirmation of dislocation breakdown, predicted theoretically in 1980[2] could be obtained experimentally so far. The dislocation breakdown is the change of an electron orbit type as a result of small angle electron-dislocation scattering, leading to a transfer of the conduction electrons from one Fermi surface sheet to another.

Tungsten single crystals with a residual resistivity ratio (RRR) of up to 80,000 and molybdenum crystals with RRR of up to 10,000 were used. The temperature and angular dependence of the transverse magnetoresistivity was measured in the temperature range from 1.5 to 40 K and in magnetic fields of up to 30 T. The dislocations were produced by compression and strain up to 4% and confirmed by electron microscopy.

We studied angular and temperature dependence of the magnetoresistivity for tungsten and molybdenum crystals before and after deformation.

In order to show that the electron-dislocation scattering may lead to intersheet transfers and, hence, to the dislocation breakdown, the following experiment was made. Two pairs of samples with their axis parallel to <100> and <110> were prepared, and a magnetic field was applied along <110> and <100>. For each sample the magnetoresistivity was measured before and after deformation, and the contribution to the magnetoresistivity due to electron-dislocation scattering was separated.

The results obtained allow us to conclude.

1. We have demonstrated that electron-dislocation scattering strongly affects the magnetoresistivity of ultra-pure tungsten and molybdenum single crystals, i.e. it changes its angular and temperature dependence.
2. A large anisotropy of the magnetoresistivity (over 1000%), caused by the electron-dislocation interaction is observed, which may be explained by an anisotropy of the quasi-orbits resulting from small angle electron-dislocation scattering.

These experimental data prove the existence of the dislocation breakdown phenomenon in tungsten and molybdenum at high magnetic fields.

References:

1 Marchenkov, V.V., *et al*., Physica B, 246-247, 476 (1998).

2 Slutskin, A.A., *et al*., Proc. All-Union Conf. On Low Temperature Physics, Kharkov, 1980, p. 241 (in Russian).

Measurement of Grain Boundary Energy in Bismuth-Bicrystals

Molodov, D.A., Institut of Physical Metallurgy und Metal Physics, RWTH Aachen, Germany

Gottstein, G., Institut of Physical Metallurgy und Metal Physics, RWTH Aachen, Germany

Heringhaus, F., NHMFL

Shvindlerman, L.S., Institute of Solid State Physics, Russian Academy of Sciences, Russia

Recently we have shown experimentally that specific grain boundaries in bismuth-bicrystals can move under the action of a magnetic driving force (*Scripta Materialia*, 37 (1997), pp. 1207-1213; *Acta Materialia*, 46 (1998), pp. 5627-5632). The driving force *p* for grain boundary motion in these experiments was provided by a magnetic field due to strong magnetic anisotropy of bismuth. Under the impact of an appropriately directed magnetic field, a free energy difference between adjacent grains is created that exerts a driving force for boundary displacement.

Realization of such scheme in experiment also provides a unique opportunity to determine the

absolute value of grain boundary surface energy. By fastening of the boundary ends on the surface of the bicrystal one balances the driving force. The driving force is provided by the capillary pressure. When the magnetic driving force is compensated by the capillary pressure of the curved boundary, the boundary motion will cease. In this case

$$p = \Delta G_m = \sigma / R\,, \qquad (1)$$

where p is the magnetic driving force for boundary displacement, ΔG_m is the difference of the magnetic free energy in both grains of the bicrystal, σ is the surface free energy of the grain boundary, R is the radius of its curvature (for 2-D situation).

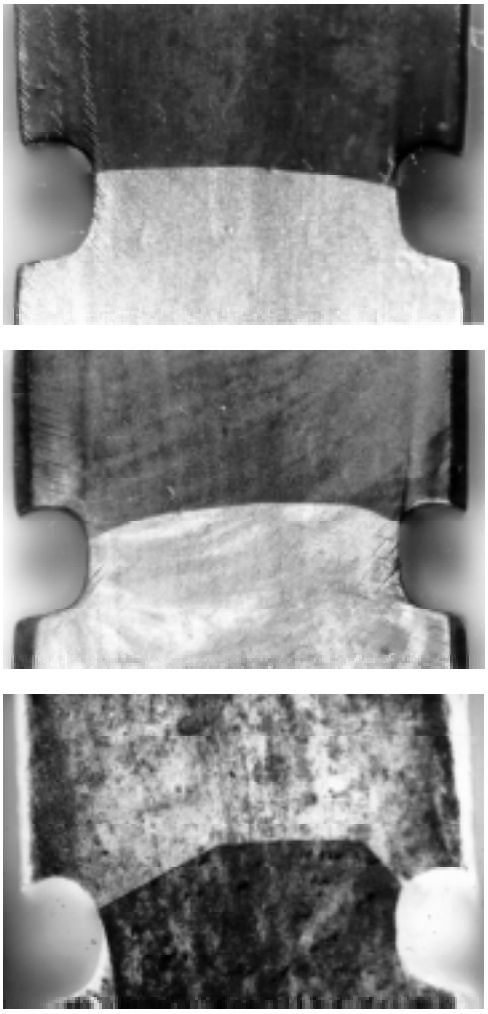

Figure 1. Grain boundary in Bi-bicrystal after annealing at 220 °C in the magnetic field of (a) $H=1.11\cdot10^7$, (b) $H=1.19\cdot10^7$, and (c) $H=1.27\cdot10^7$ A/m.

The experiments made in March 1998 showed that the notches introduced on the lateral surfaces of the samples really stopped the motion of the boundary. Figure 1 shows the shape of the investigated grain boundary after annealing in different magnetic fields. It is seen that after the annealing in the field $H=1.11\cdot10^{-7}$ A/m driving force $p = 17.0$ J/m^3), the initially straight 90°<112> tilt grain boundary became curved in the direction of the action of the driving force with radius of curvature $R=11.1 \pm 1.0$ mm (Figure 1a). An increase of the driving force leads to the phase transition "smooth curved boundary–faceted boundary," i.e. after the annealing in the fields $H=1.19\cdot10^{-7}$ A/m ($p = 245$ J/m^3) and $H=1.27\cdot10^{-7}$ A/m ($p = 279$ J/m^3) the boundary became faceted with two facets on the right and left sides and a curved segment in between (Figures 1b,c). The radius of curvature of the curved boundary segments was measured to be 8.6±1.0 mm and 11.2±1.0 mm, respectively. A calculation of the grain boundary surface energy for the curved boundary in Figure 1a and the curved segments in Figures 1b,c according to (1) gives 2.39, 2.14, and 3.14±0.02 J/m^2.

Tests of Coulomb Blockade Thermometers in High Magnetic Fields

Palm, E.C., NHMFL
Murphy, T.P., NHMFL
Hannahs, S.T., NHMFL
Pekola, J.P., Univ. of Jyväskylä, Finland
Kauppinen, J.P., Univ. of Jyväskylä, Finland

Devices with arrays of nanoscale tunnel junctions have been shown to be suitable for primary thermometry.[1] In these devices, the effect of a single electron tunneling onto an island between tunnel junctions raises its Coulomb energy, $E_c = e^2/2C_t$ where C_t is the total capacitance between the island and the environment, such that another electron cannot tunnel onto the island. In these devices the

differential conductance G(V) = dI/dV is a strongly varying function of temperature and can be used as a primary thermometer. In particular, the half width of the conductance curve $V_{1/2}$ can be written as $eV_{1/2} = 5.439Nk_BT$ and only varies with the number of junctions in the device N and the temperature T. This is of particular interest for research in high magnetic fields since the devices are fabricated from aluminum and thus should be independent of magnetic field to very high magnetic fields.

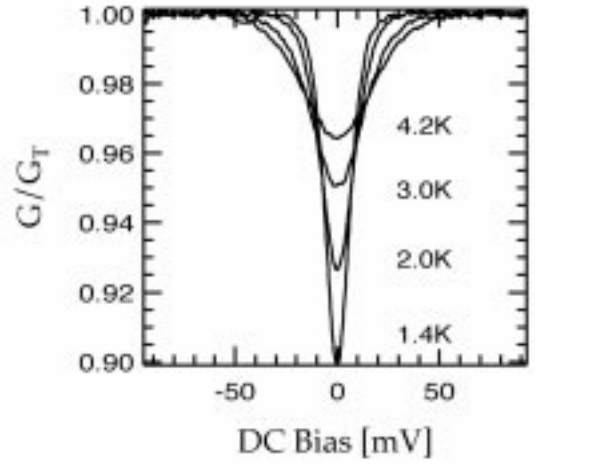

Figure 1. The normalized conductance vs. the dc voltage biased across the coulomb blockade thermometer at four different temperatures.

We have performed preliminary experiments on these devices at temperatures between 4.2 and 0.5 K and fields up to 32.5 T. The devices were measured against a calibrated germanium thermometer at zero field and compared to a capacitance thermometer at high magnetic fields. In addition, they were measured against both Cernox and RuO thermometers. A number of experimental problems were overcome. In particular, the devices were found to be very sensitive to RF pickup, thus the leads into the cryostat had to be carefully filtered. In addition, we found that changes in the temperature of the laboratory were large enough to effect the instrumentation used to measure the differential conductance and led to scatter in the derived temperatures on the order of 5%. When the instruments were thermally shielded to stabilize their temperature drift, we were able to measure the temperature of the devices with an accuracy of about 1%.

Future measurements will endeavor to precisely measure the effect of magnetic fields upon the coulomb blockade thermometers, and their subsequent suitability for primary and secondary thermometry. In addition, the measurements will also be extended to temperatures as low as 50 mK.

Reference:

1 Hirvi, K.P., *et al*., J. Low Temp. Phys, 101, 17 (1995).

Magnetic Thermometry at Low Temperatures Using LCR Meter

Shvarts, V.A., NHMFL/UF/ILTPE, Physics
Xia, J.S., NHMFL/UF, Physics
Adams, E.D., NHMFL/UF, Physics

Magnetic thermometers with paramagnetic materials as a temperature sensing substance are very useful in the low- and ultra-low range of temperatures.[1,2,3] We describe a compact and easy-to-make Cerium Magnesium Nitrate (CMN) thermometer used with a commercial automatic LCR meter.

The 0.1-g CMN pill was compressed onto 25 silver uninsolated wires clamped into a copper finger. The astatic pair pick-up coil (2×3500 turns in 17 layers of 0.001" copper wire) was wound on a 4-mm inner diameter Stycast 1266 coil former. The excitation coil (1000 turns in 4 layers of 0.002" NbTi multi-filament in copper matrix wire) was 6.2 mm inner diameter by 20 mm long. The coil assembly incapsulates the CMN pill and was surrounded by a Nb shield. The whole construction is rigid and is 10 mm outer diameter and 55 mm long.

A commercial LCR meter HP 4263B (Opt.1) was used to measure the mutual inductance M between the coils, which was proportional to the CMN susceptibility at low temperatures. Two frequencies of 100 and 1000 Hz and the lowest available excitation voltage of 20 mV were used, providing resolution of 0.1 and 0.01 μH correspondingly.

The calibration of the thermometer was performed against a ^{3}He melting pressure thermometer (MPT). The measured values of M-M_{inf}, the least-squares fit to the Curie law (left scale) and the deviations from the fit (right scale) are shown in Figure 1. Within 1% accuracy the measured susceptibility shows simple 1/T Curie behavior in the temperature range 10 mK to 100 mK. This demonstrates that:

- the linearity of the LCR meter is sufficient for use with the CMN thermometer;
- there is no significant overheating at the frequency and excitation used;
- the Weiss constant is quite small.

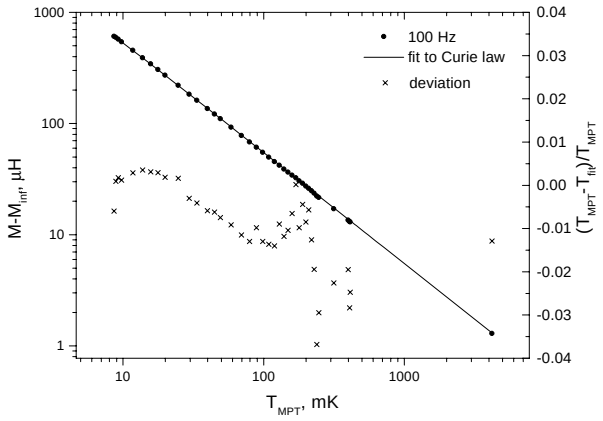

Figure 1. Mutual inductance (left) and deviation of temperature from the fit (right) vs. temperature.

Good resolution of 0.1% and reasonable intrinsic relaxation time of 15 min at 10 mK make the system attractive for many users. Moreover, the same LCR meter may be used for calibration of the CMN thermometer against superconducting fixed points and the whole calibration and measurement procedures can be easily automated.

References:

1 Greywall, D.S., *et al*., J. Low Temp. Phys., 46, 451 (1982).

2 Jutzer, M., *et al*., Z. Phys. B, 64, 115 (1986).

3 Greywall, D.S., *et al*., Rev. Sci. Instrum., 60, 471 (1989).

$NbSe_3$: High Field Magnetoresistance and Effect of Uniaxial Stress

Tessema, G.X., Clemson Univ., Physics
Gamble, B.K., Clemson Univ., Physics
Skove, M.J., Clemson Univ., Physics
Lacerda, A.H., NHMFL/LANL

We have developed a puller for the study of the effect of uniaxial stress on the electronic properties of materials with whisker-like morphology in very high (pulsed 60 T) magnetic fields. The following constitutes a successful test conducted using $NbSe_3$ whiskers.

The Fermi surface of $NbSe_3$ below the two CDW transitions is still not very clear. The giant magnetoresistance and quantum oscillations are attributed to SdH oscillations of one or more small pieces of electron or hole pockets spared by the two CDW transitions at 145 and 50 K respectively, with possibly magnetic breakdown between these pockets and the open orbits.[1,2] In a recent low field study (H < 8 T) of the transverse magnetoresistance (H in the (b,c) plane)[3] we have shown that the extremal area of one of these pockets decreases linearly with strain, ε, vanishing at ε = 2.5%. Here we extend our study into the high magnetic field regime (pulsed 60 T) and investigate the effect of uniaxial stress on the longitudinal magnetoresistance (I//H).

At low fields, H < 2 T, and H constant, R(ε,H) increases with ε, which is consistent with previous results.[3] Above 2 T, R(ε,H) decreases with increasing ε for fixed H. The results are summarized in Figure 1, which shows a plot of the magnetoresistance Δρ/ρ for ε = 0, .13, .32, .1, 1.2 %. For 10 T < H < 30 T, Δρ(ε,H)/ρ(ε,0) is linear with H for all ε. At low fields the nonlinear behavior of Δρ/ρ is suppressed by ε. The deviation from the

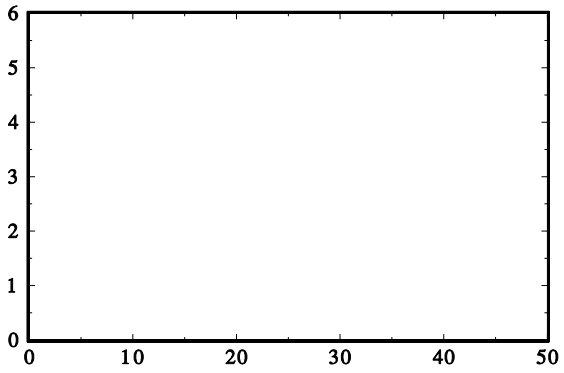

Figure 1: The strain dependence of the longitudinal magnetoresistance of $NbSe_3$.

Phase Separation in Electronic Models for Manganites

Yunoki, S., NHMFL
Hu, J., NHMFL
Malvezzi, A., NHMFL
Moreo, A., NHMFL/FSU, Physics and MARTECH
Furukawa, N., ISSP, Univ. of Tokyo
Dagotto, E., NHMFL/FSU, Physics and MARTECH

The Kondo lattice Hamiltonian with ferromagnetic Hund's coupling as a model for manganites is investigated. The classical limit for the spin of the (localized) t_{2g} electrons is analyzed on lattices of dimension 1,2,3, and ∞ using several numerical methods. The phase diagram at low temperature is presented. A regime is identified where phase separation occurs between hole-undoped antiferromagnetic and hole-rich ferromagnetic regions. Experimental consequences of this novel regime are discussed. Regions of incommensurate spin correlations have also been found. Estimations of the critical temperature in 3D are compatible with experiments.[1]

Reference:

1 Yunoki, S., *et al*., Phys. Rev. Lett. 80, 845-848 (1998).

Phase Separation Induced by Orbital Degrees of Freedom in Models for Manganites with Jahn-Teller Phonons

Yunoki, S., NHMFL
Moreo, A., NHMFL/FSU, Physics and MARTECH
Dagotto, E., NHMFL/FSU, Physics and MARTECH

The two-orbital Kondo model with classical Jahn-Teller phonons is studied using Monte Carlo techniques. The observed phase diagram is rich, and includes a novel regime of phase separation induced by the orbital degrees of freedom. Experimental consequences of our results are discussed. In addition, the optical conductivity $\sigma(\omega)$ of the model is presented. It is shown to have several similarities with experimental measurements for manganites.

Static and Dynamical Properties of the Ferromagnetic Kondo Model with a Direct Antiferromagnetic Coupling Between the Localized t_{2g} Electrons

Yunoki, S., NHMFL
Moreo, A., NHMFL/FSU, Physics and MARTECH

The phase diagram of the Kondo lattice Hamiltonian with ferromagnetic Hund's coupling in the limit where the spin of the localized t_{2g} electrons is classical, and analyzed in one dimension as a function of temperature, electronic density, and a direct antiferromagnetic coupling J´ between the localized spins. Studying static and dynamical properties, a behavior that qualitatively resembles experimental results for manganites occurs for J´/t smaller than 0.11. In particular, a coexistence of ferromagnetic and antiferromagnetic excitations is observed at low hole density in agreement with neutron scattering experiments on $La_{2-2x}Sr_{1+2x}Mn_2O_7$ with x=0.4. This effect is caused by the recently reported tendency to phase separation between hole-rich ferromagnetic and hole-undoped antiferromagnetic domains in electronic models for manganites. As J´ increases metal-insulator transitions are detected by monitoring the optical conductivity and the density of states. The magnetic correlations reveal the existence of spiral phases without long-range order, but with fairly large correlation lengths. Indications of charge ordering effects appear in the analysis of charge correlations.[1]

Reference:

1 Yunoki, S., *et al*., Phys. Rev. B 58, 6403 (1998).